Available online at www.sciencedirect.com

ScienceDirect

Ceramics International 40 (2014) 2451–2459

CERAMICS INTERNATIONAL

www.elsevier.com/locate/ceramint

Influence of rare-earth Nd, Dy, and Ho doping on structural and electrical properties of $(Na_{0.53}K_{0.47})_{0.942}Li_{0.058}NbO_3$ based lead-free piezoceramics

Jing Zhou[a,b], Qing Ma[a,c], Pengfei Wang[b], Lijin Cheng[a], Shaojun Liu[a,b,*]

[a]State Key Laboratory for Powder Metallurgy, Central South University, Changsha 410083, China
[b]Division of Materials Science and Engineering, Shenzhen Graduate School, Harbin Institute of Technology, Shenzhen 510085, China
[c]Key Laboratory of Low-carbon Energy & Energy-saving Technology, Research Institute of Tsinghua University in Shenzhen, Shenzhen 518055, China

Received 3 June 2013; received in revised form 27 July 2013; accepted 4 August 2013
Available online 9 August 2013

Abstract

Influence of larger rare-earth Nd and intermediate rare-earth Dy and Ho on the structure, doping behavior, dielectric, and piezoelectric properties of $(Na_{0.53}K_{0.47})_{0.942}Li_{0.058}NbO_3$ (KNNLN) lead-free ceramics was reported. Phase transition in KNNLN ceramics with increasing Nd, Dy, and Ho doping content occurs from the coexistence of tetragonal–orthorhombic phases to tetragonal–orthorhombic–pseudocubic phases. Both larger rare-earth Nd and intermediate rare-earth Dy and Ho ions preferentially occupy A-site and then B-site as amphoteric ions when Nd, Dy, and Ho doping content increases. Nd, Dy, and Ho doping can increase sintering density, tailor grain morphology and size, and improve piezoelectric coefficient of KNNLN ceramics. Grain size of Nd, Dy, and Ho doped KNNLN ceramics is more homogeneous and much finer than that of undoped ones. KNNLN lead-free ceramic with 2 wt% Nd doping exhibits an optimum piezoelectric coefficient (d_{33}) ~128 pCN^{-1}.

Keywords: Rare earth; Piezoceramics; Doping behavior; Lead-free

1. Introduction

Piezoceramics have a wide range of applications in the ultrasound transducer, sensor, and non-destructive testing [1]. $PbTiO_3$ and Pb(Ti, Zr)O_3 (PZT) based ceramics are the most widely studied ones [2,3]. Unfortunately, lead-based materials are harmful to human health and environment. There is an urgent need to develop a non-lead substitute to replace PZT [4]. (Na, K) NbO_3-based (KNN) ceramic is considered as one of the most promising lead-free piezoelectric ceramics because of its relatively high piezoelectric properties resulted from the existence of three separate phase boundaries [5,6].

It is well known that the existence of morphotropic phase boundaries (MPB) results in enhanced properties of lead-based piezoceramics [7]. The maximum d_{33} appears at the temperature at which the samples pass the MPB line along the temperature axis. In contrast, enhanced properties of KNN based ceramics are believed to origin from the lowering of polymorphic phase transition temperature to near room temperature [8,9]. Saito et. al [10] reported that textured and Li, Ta, and Sb co-doped KNN ceramics can exhibit comparable piezoelectricity properties with PZT ceramics, but high cost and complexity of this fabrication technique block its commercial application. Moreover, it is hard to obtain high density KNN ceramics using conventional synthesis methods because of high evaporation of K and Na at elevated sintering temperature [11]. Hence, studies of lead-free piezoelectric ceramics still focus on choosing suitable dopants and optimizing conventional ceramic fabrication technology to make high piezoelectric properties KNN ceramics, which can be further tailored by doping typical perovskite structure dielectrics [12–15], including $CaTiO_3$, $SrTiO_3$, $BiFeO_3$, $BaTiO_3$ and so on.

As the vitamin of the modern chemical industry, rare-earth (RE) oxides are known to be effective to stabilize the

*Corresponding author at: State Key Laboratory for Powder Metallurgy, Central South University, Changsha 410083, China. Tel.: +86 13974953502; fax: +86 73188876315.
E-mail address: liumatthew@csu.edu.cn (S. Liu).

0272-8842/$ - see front matter © 2013 Elsevier Ltd and Techna Group S.r.l. All rights reserved.
http://dx.doi.org/10.1016/j.ceramint.2013.08.020

temperature dependence of relative dielectric constant (ε_r) and decrease the dissipation factor (tan δ) in ferroelectric ceramics [16]. The intermediate rare-earth Dy, Ho, and Er, so-called amphoteric ions are used as dopants in $BaTiO_3$-based dielectric materials for multilayer ceramic capacitors. Rare-earth oxides are also dominant additives in forming a well developed core–shell structure in $BaTiO_3$ [17]. Additionally, rare-earth doped $PbTiO_3$, PZT, and $SrTiO_3$ have been widely studied [18,19]. It was demonstrated that Nd doping has a strong effect on the MPB and can significantly enhance the piezoelectric coefficient of PZT ceramics [20,21]. In contrast, only limited study reported on the influence of rare-earth doping on the structure and properties of KNN-based piezoelectric ceramics. Bathelt et. al [22] showed that Nd doping into $(K_{0.46}Na_{0.54})_{0.97}Li_{0.03}Nb_{0.81}Ta_{0.19}$ ceramics increases the piezoelectric response by lowering orthorhombic–tetragonal phase transition temperature. Gao et. al [23] reported that La doping into $K_{0.5}Na_{0.5}NbO_3$ ceramics effectively inhibits the grain growth and exhibits enhanced piezoelectric properties. Our preliminary results [24] showed that more homogeneous morphology and enhanced d_{33} were obtained in Nd doped $(Na_{0.53}K_{0.47})_{0.942}Li_{0.058}NbO_3$ (KNNLN) ceramics as well.

In this context, larger rare-earth Nd and intermediate Dy and Ho rare-earth were investigated to study doping behavior of Nd, Dy, and Ho and their influence on the phase transition, microstructures, dielectric, and piezoelectric properties of $(Na_{0.53}K_{0.47})_{0.942}Li_{0.058}NbO_3$ lead free based ceramics in detail.

2. Experimental procedure

Nd, Dy, and Ho doped KNNLN samples were synthesized through a conventional solid-state reaction method using reagent-grade K_2CO_3, Na_2CO_3, Li_2CO_3, Nd_2O_3, Dy_2O_3, Ho_2O_3, and Nb_2O_5 powders as raw chemicals. Before weighing, these powders were separately dried in an oven at 120 °C for 20 h. The doping content of rare-earth oxides was set as $x=0.1\%$, 0.5%, 1%, 2% and 4% in weight, respectively. Then, they were milled in nylon jars for 24 h with zirconia ball and ethanol as milling media. The weight ratio of powder, balls and alcohol was set as 1:1.2:3. After as-milled powders were transferred to alumina crucible for calcination at 750 °C for 3 h in air, they were re-milled, dried, and pressed into disks of 10 mm in diameter and 3 mm in thickness using PVA as a binder. Cold isostatic pressing was further used to achieve high and homogeneous pressing density. After pellets were heated at 500 °C for 30 min to completely burn off the binder, they were sintered at 1080 °C for 3 h in air with a heating rate of 5 °C/min. Density of KNN based samples was measured by volume–weight means.

The crystal structure of as-sintered samples was determined by a high resolution X-ray diffractometer (XRD) (Rigaku D/max 2500Pc) using Cu K_α with a 1.540562 Å wavelength. XRD measurements were taken in the range of 2θ from 10 to 90 °C with scanning rate of 1°/min and step size of 0.02°. Raman spectra were attained by Micro-Raman Spectroscopy (Renishaw InVia Reflex) using 514.5 nm Ar^+ blue laser as exciting source. Raman Spectroscopy scanned the polished surface of pellets on the range of wave number from 1000 cm^{-1} to 100 cm^{-1}. Scanning electron microscopy (SEM) (Hitachi S-4700) was employed to observe the microstructure and morphology of as-sintered ceramics.

As-sintered samples were polished to ensure smooth surface. Silver paste was painted on both surfaces and fired at 800 °C for 10 min in air to form the electrodes for electrical measurement. Capacitance and loss tangents were measured using an Aglient E4980A meter at 10 KHz. The dielectric constant (ε_r) was calculated from the measured capacitances, thickness, and electrode area of samples. The variation of dielectric constant with temperature was measured at the temperature from 25 °C to 550 °C. For piezoelectric measurement, the samples were immersed in silicon oil and poled in a 30 kv/cm direct current electric field at 130 °C for 30 min. Piezoelectric coefficient d_{33} was measured by a quasistatic piezoelectric constant testing meter (Model ZJ-3).

3. Results and discussion

3.1. XRD patterns

XRD patterns of Nd doped $(Na_{0.53}K_{0.47})_{0.942}Li_{0.058}NbO_3$ (KNNLN) ($x=0.1$ wt%, 0.5 wt%, 1 wt%, 2 wt% and 4 wt%) ceramics sintered at 1080 °C for 3 h in air are shown in Fig. 1(a). Nd-doped ceramics are of single perovskite structure without detectable secondary phases within the sensitivity of XRD, indicating that the solid solubility limit of Nd_2O_3 into KNNLN is larger than 4 wt%. It is well known that Li^+ ions are supposed to substitute A-site of Na^+ and K^+ in KNN ceramics, leading to crystal structure change of KNN solid solution from orthorhombic system to tetragonal one due to large distortion caused by Li^+ [25]. In a consistent with previous reports, tetragonal and orthorhombic phases coexist in undoped KNNLN ceramics [26]. When $x=0.5$ wt%, orthorhombic phase becomes dominant. Pseudocubic phase begins to appear in $x=1$–1.5 wt% Nd doped ceramics.

To further analyze the influence of Nd doping on the phase structure of ceramics, XRD analysis was performed in the range of 2θ from 44° to 65°. Fig. 2(a) shows the corresponding expanded XRD patterns of Nd doped samples in the range of 2θ from 44° to 65°. As shown in Fig. 2(a), the splitting between two diffraction peaks near 57° gradually disappears as Nd doping content is above 2 wt%, seemly indicating that the dominant orthorhombic phase transforms to pseudocubic phase. However, it is shown by Raman spectra analysis below that both tetragonal and orthorhombic phases still reserve in 4 wt% Nd doped ceramics.

It is noticed that XRD peaks of Nd-doped KNNLN with $x\leqq 2$ wt% shift towards higher angle. According to Shannon's effective ionic radii with a coordination number of six, the radius of Nd^{3+} ($r=0.983$ Å) is smaller than that of Na^+ (1.02 Å) and K^+ (1.33 Å) [27]. We believe that the radius effect is presumably responsible for the steady shift of the

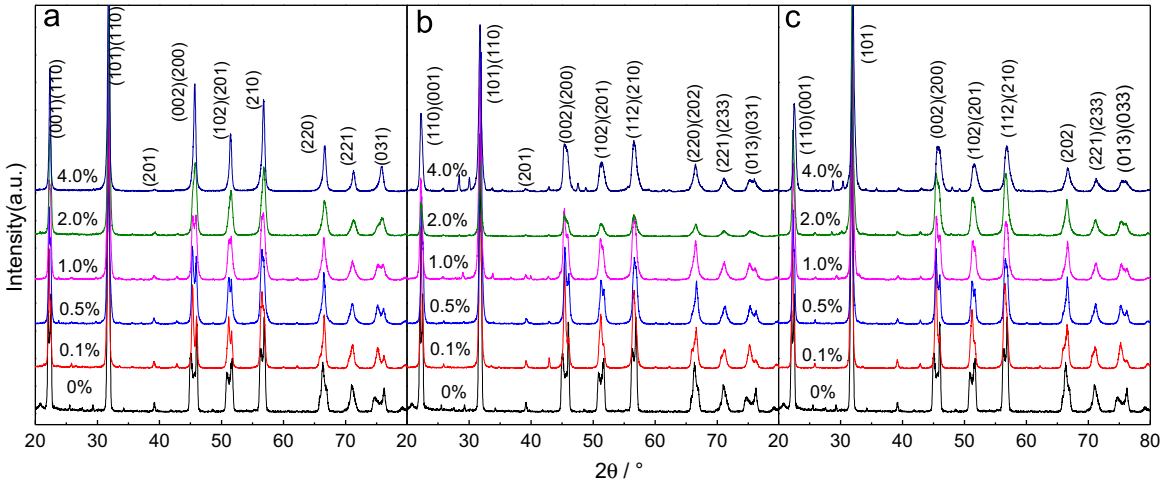

Fig. 1. XRD patterns measured in the range of 2θ from 10 °C to 90 °C of (a) Nd, (b) Dy, and (c) Ho doped $(Na_{0.53}K_{0.47})_{0.942}Li_{0.058}NbO_3$ ceramics at room temperature, showing an appearance of traces of secondary phases evidenced by extra peaks at near (110) and (101) peaks in 1 wt% Ho and Dy doped $(Na_{0.53}K_{0.47})_{0.942}Li_{0.058}NbO_3$ ceramics. Note: Nd, Dy, and Ho doping content was set as x=0.1%, 0.5%, 1%, 2% and 4% in weight.

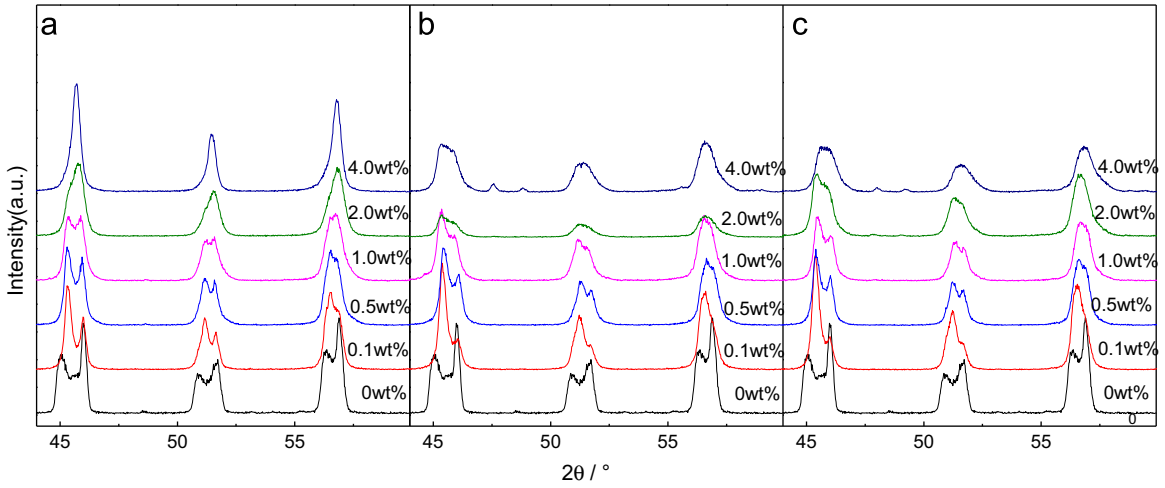

Fig. 2. Enlarged XRD patterns in the range of 2θ from 44 °C to 65 °C of (a) Nd, (b) Dy, and (c) Ho doped $(Na_{0.53}K_{0.47})_{0.942}Li_{0.058}NbO_3$ ceramics at room temperature, showing that the splitting between two diffraction peaks near 57° gradually disappears as Nd, Dy and Ho doping content above 2 wt% ceramics.

XRD peaks to higher angle with increasing Nd_2O_3 doping. However, XRD peaks of Nd-doped KNNLN samples with $x > 2$ wt% turn to shift to lower angle. It is well known that rare-earth ions can incorporate into both A- and B sites in $BaTiO_3$ based ceramics. They preferentially occupy A-site and then B-site as doping content increases, assuming that the local strain is similar in both A- and B-sites in $BaTiO_3$. The substitution of rare-earth ions into Nb^{5+} site results in the peaks shifting to lower angle due to larger radius of Nd^{3+} than that of Nb^{5+}, a fact that is confirmed by Raman spectra below.

Fig. 1(b) and (c) shows the XRD patterns of Dy-doped and Ho-doped samples, respectively. In contrast, Fig. 2(b) and (c) shows the corresponding expanded XRD patterns of Dy and Ho doped ceramics in the range of 2θ from 44° to 65°, respectively. As shown, when Dy and Ho doping content is in the range of 0.1–1 wt%, the peak near 46° in Fig. 2(b) and (c) indicates that the dominant phase is still orthorhombic. Similar to phase transitions occurred in Nd-doped ceramics, the splitting peaks in 2 wt% Dy and Ho doped samples almost emerge, an indicative of the appearance of pseudocubic phase. Again Raman spectra below show that tetragonal and orthorhombic phases still exist. With increasing Dy and Ho doping, the crystal structure of ceramics are changed from the coexistence of tetragonal and orthorhombic phases to tetragonal, orthorhombic, and pseudocubic phases. However, unidentified secondary phases begin to appear at both 0.5–1 wt% Ho and Dy doped KNNLN, which become especially obvious when the doping content of Dy and Ho is 4 wt%. This implies that the solid solubility limit of Dy and Ho incorporated into KNNLN lattice sites is lower than 0.5–1 wt%.

Generally, the energy needed for the incorporation of a dopant ion at an individual lattice site in complex oxide is related to lattice distorting, which is dominated by the difference in ionic radii, the formation energy of compensating defects, and polarization energy during the incorporation of ions [17]. In contrast, the extent of a dopant ion in a host structure of the solid solution

depends on the site where dopant ion is substituted into and the compensation mechanism. The difference in ionic size is usually considered as a main factor influencing the incorporation of rare-earth ions into oxides. The radius of Nd^{3+} (r=0.983 Å), Dy^{3+} (r=0.912 Å), and Ho^{3+} (r=0.901 Å) is much larger than that of Nb^{5+} (0.64 Å). In contrast, their radius is closer to that of Na^{+} (1.02 Å) [27]. Therefore, from the viewpoint of crystal chemistry, Nd^{3+}, Dy^{3+}, and Ho^{3+} ions most likely enter A-site to substitute Na^{+} ions as donor-type dopants compensated by oxygen vacancies due to less lattice distortion and energy needed for the substitution of A-site rather than B-site. Moreover, it is expected that the solution solubility limit of Nd doping into KNNLN is the highest among Nd^{3+}, Dy^{3+}, and Ho^{3+} again due to less lattice distortion since the radius of Nd^{3+} (r=0.983 Å) is closest to that of A-site Na^{+} and K^{+}. Similar to previous report on $BaTiO_3$ ceramics [16], our results show that the solid solubility limit of Dy and Ho in the KNN structure is similar due to their similar ionic size. It should be stressed that excess rare-earth oxides may compensate the loss of Na and K by diffusing into A-site during elevated sintering temperature.

3.2. Raman spectra

Since vibrations of NbO_6 octahedron in KNN-based systems are sensitive to occurrence of phase transitions and tetragonal phase, Raman spectroscopy was used to further determine the structure change of KNNLN samples. Usually, there are strong broad lines near 260 cm^{-1} (A1) and 615 cm^{-1} (A2) and a weaker line near 860 cm^{-1} (A3) [28]. The lower frequency A1 and A2 modes in the Raman spectra represent the double degenerate symmetric O–Nb–O stretching vibration and the triply degenerate symmetric O–Nb–O bending vibration of NbO_6 octahedra in KNN ceramics, respectively [29]. Additionally, there is a distinct shoulder on the low-frequency sides of A2 mode in the orthorhombic and tetragonal KNN based phases, although the intensity of shoulder present in the tetragonal phase is rather weaker.

Fig. 3 shows the Raman spectra of Nd, Dy, and Ho doped KNNLN ceramics. It is observed that the similarity between the Raman spectra of the samples with different Nd, Dy, and Ho doping content is very strong. As shown in Fig. 3(a), the shoulder at the low-frequency side near 618 cm^{-1} broadens and its intensity decreases with increasing Nd content, implying a clear signal of disorder resulting from the tetragonal distortion in KNNLN ceramics with increasing Nd content. However, the existence of weaker line near 863 cm^{-1} suggests that tetragonal phase still exists when Nd doping content is 4 wt%. It is noticeable that no obvious shifting of A1, A2, and A3 modes for Nd doped KNNLN in the range of x=0–2 wt% was observed. The change in the peak positions of the Raman spectra is usually accompanied with large changes in the sample's optical properties and Raman scattering intensity. It was reported that the frequency does not show obvious change in $K_{0.5}Na_{0.5}NbO_3$ and $BaTiO_3$ ceramics with tetragonal–orthorhombic phase transition process when the temperature continues increasing to a critical value, which can be defined as a temperature of diffusion phase transition from orthorhombic to tetragonal phase [30]. In addition to suggesting that Nd prefers to substitute into A-site of KNNLN based ceramics, very slight shifting of peak position of A1 and A2 modes implies that a diffusion phase transition from tetragonal to orthorhombic phase occurs until tetragonal phase is dominant.

It is of particular interest to observe that A1 and A2 modes, which represent the double degenerate symmetric O–Nb–O stretching vibration and the triply degenerate symmetric O–Nb–O bending vibration of NbO_6 octahedra in KNNLN ceramics with >2 wt% Nd doping, respectively, shift downwards. This implies that the O–Nb–O bond angle changes as a result of Nd^{3+} substitution into Nb^{5+} sites. Weaker interaction of larger radius of Nd^{3+} ion with the anions is responsible for the downward shifting of the frequency. Moreover, this downward shifting of the samples with high Nd doping content also indicates a weaker bonding between the cations and the anions.

In a combination with the XRD results, phase transition in KNNLN based ceramics with increasing Nd doping content occurs from coexistence of tetragonal–orthorhombic phases to tetragonal–orthorhombic–pseudocubic phases. We would like

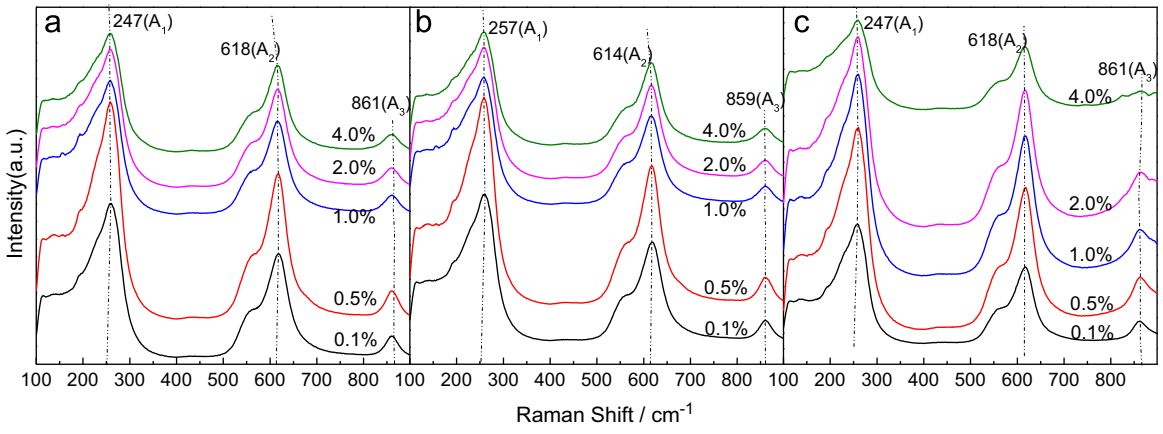

Fig. 3. Room temperature Raman spectra of (a) Nd, (b) Dy, and (c) Ho doped $(Na_{0.53}K_{0.47})_{0.942}Li_{0.058}NbO_3$ ceramics on the range of wave number from 1000 cm^{-1} to 100 cm^{-1}. Note: the doping content of Nd, Dy, and Ho was set as x=0.1%, 0.5%, 1%, 2% and 4% in weight.

to mention that when ambient temperature is near the critical temperature of tetragonal–orthorhombic phase transition, phase structure will be very sensitive to the composition inhomogeneity, which usually occurs in oxide ceramics. A study of KNN based ceramic by XRD suggested that rhombohedra–orthorhombic phase transition is inhomogeneous, initiated by islands of rhombohedral material within an orthorhombic matrix, with phase transition completed only after the coalescence islands form [31].

Fig. 3(b) and (c) shows the Raman spectra for Dy doped and Ho doped KNNLN ceramics, respectively. Phase transition occurring in Dy and Ho doped ceramics is very similar to that in Nd doped ceramics, as observed that all three modes (A1, A2, and A3) for Dy and Ho doped ceramics have a similar Raman shifting to those of Nd doped ones. It is further observed that A1 mode, A2 mode, and shoulders at the low-frequency side of A2 mode of Dy and Ho doped ceramics broaden and their intensity becomes weak with increasing Dy and Ho content. Again no obvious shifting of the A1, A2, and A3 frequencies was observed, when Dy and Ho content is in a range of 0–2 wt%. In contrast, A1 and A2 modes for ceramics with Dy and Ho doping content >2 wt% shift downwards, again an indicative of Dy^{3+} and Ho^{3+} substitution into Nb^{5+}. In addition to appearance of secondary phase as shown in XRD patterns, phase transition in Dy and Ho doped KNNLN ceramics occurs from coexistence of tetragonal–orthorhombic phases to tetragonal–orthorhombic–pseudocubic phases with increasing doping as well.

3.3. Sintering density and microstructure

The dependence of sintering density on Nd, Dy, and Ho doping content for KNNLN ceramics is shown in Fig. 4. Overall, the sintering density significantly increases with >0.5 wt% Nd, Dy, and Ho doping content, but Nd doped KNNLN ceramics shows relatively higher sintering density. Especially, when Nd doping content in KNNLN ceramics reaches up to 4 wt%, its relative density increases from ~86.5% (undoped) to ~92%.

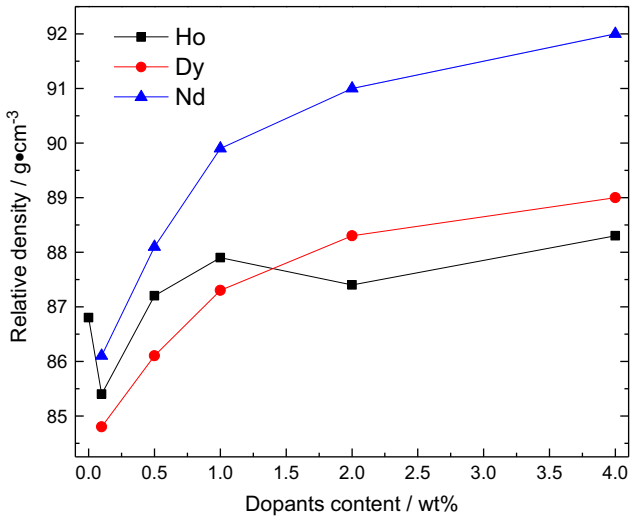

Fig. 4. Relative sintering density of Ho, Dy, and Nd doped $(Na_{0.53}K_{0.47})_{0.942}Li_{0.058}NbO_3$ ceramics sintered at 1080 °C for 3 h in air with a heating rate of 5 °C/min.

Fig. 5 shows SEM images of as-sintered Nd, Dy, and Ho doped KNNLN ceramics. All the samples consist of stacked plates with square or rectangular grains. Previous reports showed that systems with nonisotropic interfacial energy can adopt plate-like grains when a small amount of liquid phase related to Na_2O volatilization in KNN based ceramics appears [32]. In this case, grains undergo considerable changes in shape and develop a morphology in which contacting regions between neighboring grains are relatively flat [33]. As shown in Fig. 5(a), the grains of undoped samples with the average grain size 2.5–10 μm are least homogeneous with a number of abnormal grains. Abnormal grain growth controlled by diffusion in KNNLN ceramics is also believed to be related with the formation of liquid phase. With increasing Nd doping content, size of the square or rectangular grains significantly decrease. When Nd doping content is 2 wt%, random-shaped grains with much finer grain size become dominant. Similar results have been reported for La-doped KNN [23], PZT [34], and BNT ceramics [35]. Donor doping usually leads to an inhibition of grain growth as observed in PZT-based ceramics by reducing the diffusion coefficient since A-site vacancies created by doping are supposed to be bound to the doping ion [36]. This results in weakened mass transportation and inhibited grain growth. It is reasonable that KNNLN based ceramics can adopt this similar mechanism.

However, obvious abnormal grain growth is observed again in 4 wt% Nd doped KNNLN ceramics. Its origin is still not clear, but Ahn et. al [32] pointed out that the fraction control of liquid phase is an important factor to obtain uniform microstructure in KNN based ceramics. Another possibility is resulted from oxygen vacancies induced by B-site substitution of Nd to keep the charge neutrality in 4 wt% Nd doped ceramics, which is a well-known point defect to favorite the atom diffusion during the sintering processing [37]. Raman spectra results above clearly show that B-site substitution occurs when Nd doping content is larger than 2 wt%. Moreover, the formation of liquid phase can be suppressed with increasing Nd doping content, which compensates the loss of Na and K evaporation during the elevated sintering temperature.

Very similar microstructure and square or rectangular grain evolution occurs in Dy and Ho doped KNNLN ceramics, as shown in Fig. 5(e)–(j). The average grain sizes of Dy-doped KNNLN ceramics with $x=0.1$ wt%, 0.5 wt%, 1 wt%, 2 wt%, and 4 wt% is ~0.8 μm, ~1.0 μm, ~0.8 μm, ~0.8 μm, and ~0.6 μm, respectively. In contrast, the average grain sizes of Ho-doped KNNLN with $x=0.1$ wt%, 0.5 wt%, 1 wt%, 2 wt% and 4 wt% are ~1.5 μm, ~1.5 μm, ~1.0 μm, ~1.0 μm and ~0.8 μm, respectively. Especially, the average grain size of Dy and Ho doped KNNLN ceramics is much finer and more homogeneous compared to that of Nd doped ones. However, it is noticeable that there is no abnormal grain growth in 4 wt% Dy or Ho doped KNNLN ceramics. The inhibited grain growth

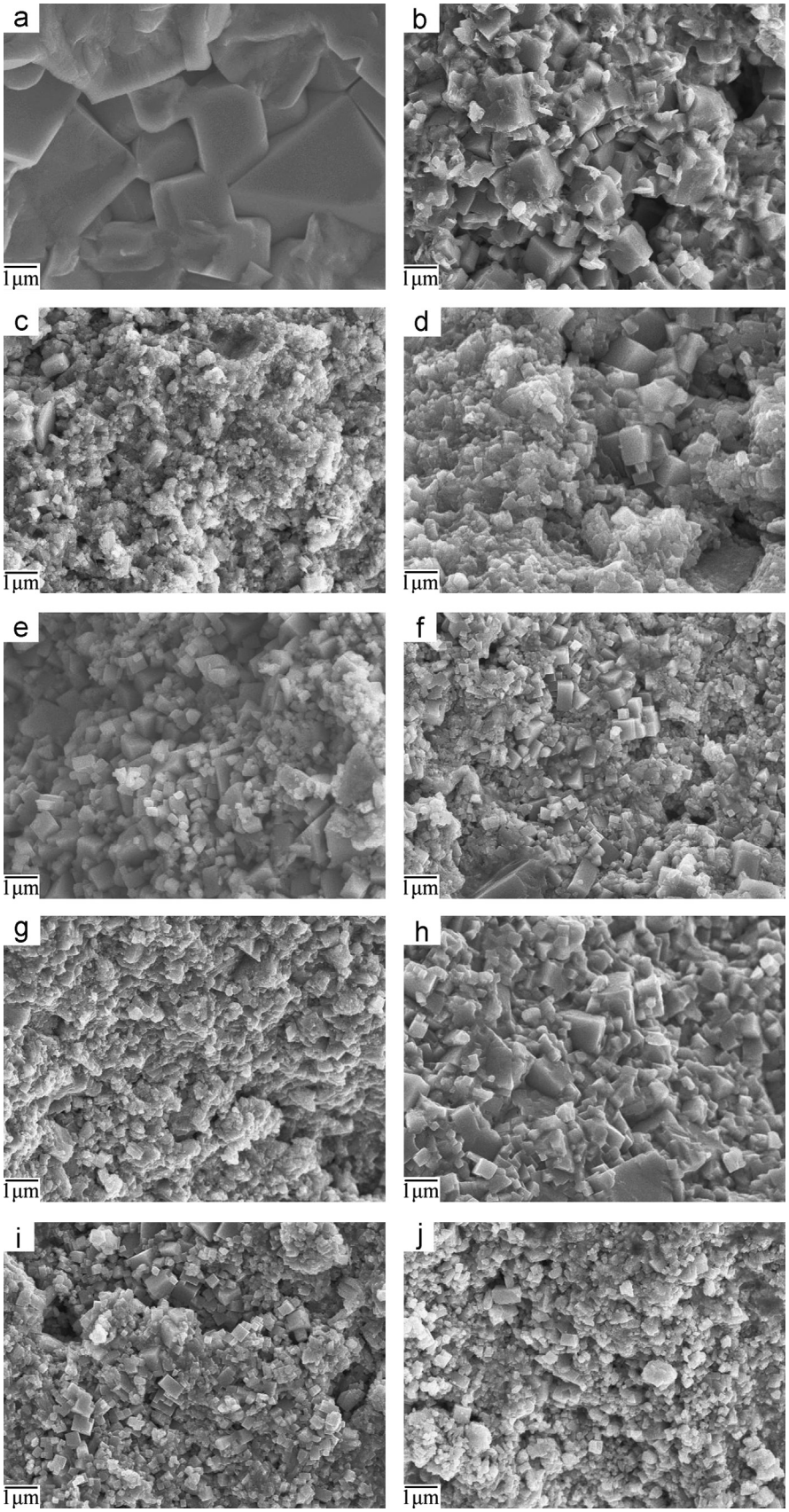

Fig. 5. SEM images of (a) undoped, (b) 0.1 wt% Nd, (c) 2 wt% Nd, (d) 4 wt% Nd, (e) 0.1 wt% Dy, (f) 2 wt% Dy, (g) 4 wt% Dy, (h) 0.1 wt% Ho, (i) 2 wt% Ho, and (j) 4 wt% Ho doped $(Na_{0.53}K_{0.47})_{0.942}Li_{0.058}NbO_3$ ceramics sintered at 1080 °C for 3 h in air with a heating rate of 5 °C/min.

is partly due to the appearance of secondary phase in KNNLN ceramics with over 2 wt% Dy and Ho doping content, as shown in XRD patterns. It is well known that the segregation of secondary phases at grain boundaries can effectively inhibit grain growth.

3.4. Dielectric and piezoelectric properties

The temperature dependence of relatively dielectric constant (ε_r) of Nd, Dy, and Ho doped KNNLN based ceramics measured at 10 KHz are shown in Fig. 6. All the samples exist a sharp peak between 400 and 420 °C, which is defined as Curie point (T_c). Relative dielectric constants (ε_r and $\varepsilon_{T\text{-}C}$), dielectric loss (D_r), Curie point (T_c), and d_{33} of Nd, Dy, and Ho doped ceramics are further summarized in Table 1. We do not observe change trend of ε_r. There are several facts that can be ascribed to this change in ε_r at room temperature. Firstly, it becomes more complicated when orthorhombic–tetragonal (O–T) phase transition in KNNLN ceramics occurs at near room temperature. Secondly, it is well known that the finer grain size can increase ε_r but secondary phases decrease ε_r. However, compared to undoped KNNLN with ε_r=545, significantly enhanced dielectric constant at room temperature in several Nd, Dy, and Ho doped samples were observed. For example, ε_r at room temperature of 1 wt% Nd doped, 2 wt% Nd doped, and 1 wt% Ho doped ceramics are 749, 696, and 807, respectively. In contrast, it seems to be comparatively insensitive to the doping of Dy_2O_3.

Fig. 7 shows the piezoelectric constant (d_{33}) of Nd, Dy, and Ho doped KNNLN ceramics as a function of Nd, Dy, and Ho doping content. As shown, Nd, Dy, and Ho doping can increase d_{33} value of KNNLN ceramics. It is more significant when Nd, Dy, and Ho doping content is >1 wt%. However, Nd doped KNNLN ceramics exhibits relatively higher d_{33} value than Dy and Ho doped counterparts. The observed d_{33} for 2 wt% Nd doped ceramics is increased to $\sim$128 pCN^{-1} from $\sim$87 pCN^{-1} for undoped ones. There are several reasons that can be ascribed to the enhancement of d_{33}. As mentioned above, excessive doping can compensate the loss of evaporative K and Na at elevated sintering temperature. It was found that A-site deviation from stoichiometry in KNN based ceramics can significantly degrade the piezoelectric properties [6]. It was reported that the piezoelectric coefficient d_{33} values tend to decline when abnormal grains appear [38]. In contrast, a sound grain growth can result in a consummate development of ferroelectric domains and thus improves the piezoelectric properties [39]. As shown in Figs. 4 and 5 respectively, 2 wt% Nd doped KNNLN ceramics shows more homogeneous grains and relatively high sintering density. Similar to an MPB composition, a maximum d_{33} is expected owing to the summation of possible crystallographic orientations. The coexistence of orthorhombic–tetragonal–pseudocubic phases makes 2 wt% Nd doped KNNLN ceramics

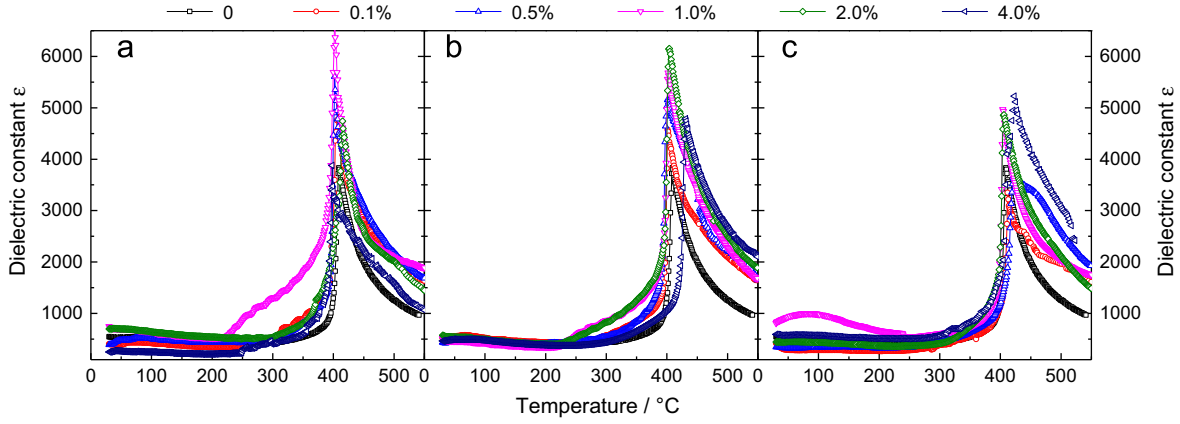

Fig. 6. Temperature dependence of dielectric constant for (a) Nd, (b) Dy, and (c) Ho doped $(Na_{0.53}K_{0.47})_{0.942}Li_{0.058}NbO_3$ ceramics measured at 10 KHz and at the temperature from 25 °C to 550 °C.

Table 1
Dielectric constant (ε_r), dielectric loss (tan δ), Curie points (Tc and TT-c), and piezoelectric coefficient (d_{33}) of Ho, Dy, and Nd doped $(Na_{0.53}K_{0.47})_{0.942}Li_{0.058}NbO_3$ ceramics.

Doped	Nd					Dy					Ho				
x (%)	ε_r	$\varepsilon_{C\text{-}T}$	tan δ	T_c (°C)	d_{33}	ε_r	$\varepsilon_{C\text{-}T}$	tan δ	T_c (°C)	d_{33}	ε_r	$\varepsilon_{C\text{-}T}$	tan δ	T_c (°C)	d_{33}
0	545	3830	0.169	412	87	545	3830	0.169	412	87	545	3830	0.169	412	87
0.1	403	5133	0.129	405	82	520.7	4574	0.15	405	78	416	3348	0.122	413	68
0.5	391	5608	0.205	406	84	434.7	5154	0.139	406	83	344	3679	0.085	422	71
1	749	5931	0.081	406	93	515.7	5684	0.154	406	106	807	4968	0.036	404	82
2	696	4740	0.144	417	128	575.7	6154	0.147	408	90	433	4865	0.034	407	97
3	247	3870	0.169	400	117	466	4787	0.234	433	97	591	5228	0.299	424	92

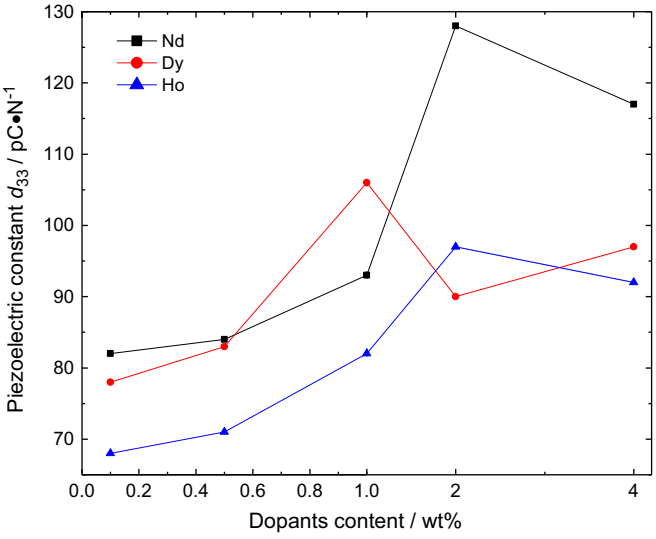

Fig. 7. Dependence of piezoelectric constant (d_{33}) of $(Na_{0.53}K_{0.47})_{0.942}$-$Li_{0.058}NbO_3$ ceramics on Nd, Dy, and Ho doping content measured at room temperature.

possess more possible polarization states at near room temperature.

4. Conclusion

With increasing Nd, Dy, and Ho doping content, phase transition of KNNLN ceramics changes from the coexistence of tetragonal–orthorhombic phases to tetragonal–orthorhombic–pseudocubic phases. Both larger rare-earth Nd and intermediate Dy and Ho ions preferentially occupy A-site and then B-site as amphoteric ions when the doping content increases. As effective grain growth inhibitor, rare earth doping can significantly increase sintering density and effectively tailor grain morphology and size of KNNLN ceramics. Grain size of Nd, Dy, and Ho doped KNNLN ceramics is more homogeneous and much finer than that of undoped KNNLN ceramics. KNNLN based ceramic with 2 wt % Nd doping exhibits an optimum piezoelectric coefficient ($d_{33}=128$ pCN^{-1}) with dielectric constant (ε_r) 696 at room temperature.

Acknowledgments

This work was financially supported by the Program for the National Natural Science Foundation of China (Grant no. 51172053) and the Science Research Funding of Shenzhen Municipality (Grant no. JC201105160545A).

References

[1] M.D. Maeder, D. Damjanovic, N. Setter, Lead free piezoelectric materials, Journal of Electroceramics 13 (2004) 385–392.
[2] X. Chen, K. Jiang, Z.G. Hu, X.F. Chen, G.S. Wang, X.L. Dong, et al., Abnormal electronic transition variations of lanthanum-modified lead zironate stannate titanate ceramics near morphotropic phase boundary: a spectroscopic evidence, Applied Physics Letters 101 (2012) 011914.
[3] L. Bellaiche, A. Garcia, D. Vanderbilt, Finite-temperature properties of $Pb(Zr,Ti)O_3$ alloys from first principles, Physical Review Letters 84 (2000) 5427–5430.
[4] J. Roedel, W. Jo, K.T.P. Seifert, E.M. Anton, T. Granzon, D. Damjanovic, Perspective on the development of lead-free piezoceramics, Journal of the American Ceramic Society 92 (2009) 1153–1377.
[5] J.J. Zhou, J.F. Li, L.Q. Cheng, K. Wang, X.W. Zhang, Q.M. Wang, Addition of small amounts of $BiFeO_3$ to $(Li,K,Na)(Nb,Ta)O_3$ lead-free ceramics: influence on phase structure, microstructure and piezoelectric properties, Journal of the European Ceramic Society 32 (2012) 3575–3582.
[6] S.J. Liu, B.B. Wan, P.F. Wang, S.H. Song, Influence of A-site nonstoichiometry on structure and electrical properties of $K_{0.5}Na_{0.5}NbO_3$ based lead-free piezoelectric ceramics, Scripta Materialia 63 (2010) 124–127.
[7] B. Noheda, Structure and high-piezoelectricity in lead oxide solid solutions, Current Opinion in Solid State and Materials Science 6 (2002) 27–34.
[8] S.C. Bhatt, M. Uniyal, Synthesis, characterization and dielectric properties of $K_{1-x}Na_xNbO_3$, International Journal of Materials and Chemistry 2 (2012) 47–50.
[9] P. Kumar, M. Pattanaik, Sonia, Synthesis and characterizations of KNN ferroelectric ceramics near 50/50 MPB, Ceramics International 39 (2013) 65–69.
[10] Y. Saito, H. Takao, T. Tani, T. Nonoyama, K. Takatori, T. Homma, et al., Lead-free piezoceramics, Nature 432 (2004) 84–87.
[11] U. Flückger, H. Arend, On the preparation of pure, doped and reduced $KNbO_3$ single crystals, Journal of Crystal Growth 43 (1977) 406–416.
[12] I.T. Seo, K.H. Cho, H.Y. Park, S.J. Park, M.K. Choi, S. Nahm, et al., Effect of CuO on the sintering and piezoelectric properties of 0.95$(Na_{0.5}K_{0.5})NbO_3$–0.05$SrTiO_3$ lead-free piezoelectric ceramics, Journal of the American Ceramic Society 91 (2008) 3955–3960.
[13] D. Lin, K.W. Kwok, HWL Chan, Effects of MnO_2 on the microstructure and electrical properties of 0.94$(K_{0.5}Na_{0.5})NbO_3$–0.06$Ba(Zr_{0.05}Ti_{0.95})O_3$ lead-free ceramics, Materials Chemistry and Physics 109 (2008) 455–458.
[14] S.J. Zhang, R. Xia, T.R. Shrout, Modified $(K_{0.5}Na_{0.5})NbO_3$ based lead free piezoelectrics with broad temperature usage range, Applied Physics Letters 91 (2007) 132913.
[15] J.G. Wu, D.Q. Xiao, Y.Y. Wang, W.J. Wu, B. Zhang, J.G. Zhu, $CaTiO_3$-modified $(K_{0.5}Na_{0.5})(Nb_{0.96}Sb_{0.04})O_3$ lead-free piezoelectric ceramics, Journal of the American Ceramic Society 91 (2008) 3402–3404.
[16] C.H. Kim, K.J. Park, Y.J. Yoon, M.H. Hong, J.O. Hong, K.H. Hur, Role of yttrium and magnesium in the formation of core–shell structure of $BaTiO_3$ grains in MLCC, Journal of the European Ceramic Society 28 (2008) 1213–1219.
[17] K.J. Park, C.H. Kim, Y.J. Yoon, S.M. Song, Y.T. Kim, K.H. Hur, Doping behaviors of dysprosium, yttrium and holmium in $BaTiO_3$ ceramics, Journal of the European Ceramic Society 29 (2009) 1735–1741.
[18] Y. Sakabe, Y. Hamaji, H. Sano, N. Wada, Effects of rare-earth oxides on the reliability of X7R dielectrics, Japanese Journal of Applied Physics 41 (2002) 5668–5679.
[19] D. Makovec, Z. Samardzija, M. Drofenik, Solid solubility of holmium, yttrium, dysprosium in $BaTiO_3$, Journal of the American Ceramic Society 87 (2004) 1324–1329.
[20] Z.G. Zhu, G.R. Li, B.S. Li, et al., The influence of Yb and Nd substituents on high-power piezoelectric properties of PMS–PZT ceramics, Ceramics International 34 (2008) 2067–2072.
[21] C.A. Randall, N. Kim, J.P. Kuchera, W. Cao, T.R. Shrout, Intrinsic and extrinsic size effects in fine-grained morphotropic phase boundary lead zirconate titanate ceramics (PZT: Nb), Journal of the American Ceramic Society 81 (1998) 677–688.
[22] R. Bathelt, T. Soller, K. Benkert, C. Schuh, A. Roosen, Neodymium doping of KNNLT, Journal of the European Ceramic Society 14 (2012) 3767–3772.

[23] D.J. Gao, K.W. Kwok, D.M. Lin, H.L.W. Chan, Microstructure and electrical properties of La-modified $K_{0.5}Na_{0.5}NbO_3$ lead-free piezoelectric ceramics, Journal of Physics D: Applied Physics 42 (2009) 035411.
[24] S.J. Liu, P.F. Wang, B.B. Wan, Q. Ma, Structural and electrical properties of Nd doped $K_{0.53}Na_{0.47}NbO_3$ based lead-free piezoceramics, Chinese Journal of Nonferrous Metals 22 (2012) 2010–2015.
[25] K. Guo, Kakimoto, H. Ohsato, Phase transitional behavior and piezoelectric properties of $(Na_{0.5}K_{0.5})NbO_3$–$LiNbO_3$ ceramcis, Applied Physics Letters 85 (2004) 4121–4123.
[26] P. Zhao, B.P. Zhang, R. Tu, T. Goto, High piezoelectric d_{33} coefficient in Li/Ta/Sb–codoped lead–free (Na,K)NbO_3 ceramics sintered at optimal temperature, Journal of the American Ceramic Society 91 (2008) 3078–3081.
[27] R.D. Shannon, Revised effective ionic radii and systematic studies of interatomic distances in halides and chalcogenides, Acta Crystallographica A 32 (1976) 751–767.
[28] H.J. Trodahl, N. Klein, D. Damjanovic, N. Setter, B. Ludbrook, D. Rytz, et al., Raman spectroscopy of (K, Na)NbO_3 and (K, Na)$_{1-x}Li_xNbO_3$, Applied Physics Letters 93 (2008) 262901–262903.
[29] N. Klein, E. Hollenstein, D. Damjanovic, H.J. Trodahl, N. Setter, M. Kuball, A study of the phase diagram of (K, Na, Li)NbO_3 determined by dielectric, piezoelectric measurements, and Raman spectroscopy, Journal of Applied Physics 102 (2007) 014112.
[30] J.A. Baier-Saip, E. Ramos-Moor, A.L. Cabrera, Raman study of phase transitions in $KNbO_3$, Solid State Communications 135 (2005) 367–372.
[31] Y.J. Dai, X.W. Zhang, G.Y. Zhou, Phase transitional behavior in $K_{0.5}Na_{0.5}NbO_3$–$LiTaO_3$ ceramics, Applied Physics Letters 90 (2007) 262903–262905.
[32] C.W. Ahn, C.S. Park, C.H. Choi, S. Nahm, M.J. Yoo, H.G. Lee, Sintering behavior of lead-free (K, Na)NbO_3-based piezoelectric ceramics, Journal of the American Ceramic Society 92 (2009) 2033–2038.
[33] J.S. Reed, Principles of Ceramic Processing, 2nd ed., Wiley-Interscience, New York, 1995.
[34] M. Laurent, U. Schreiner, P.A. Langjahr, A.E. Glazounov, M.J. Hoffmann, Microstructural and electrical characterization of La-doped PZT ceramics prepared by a precursor route, Journal of the American Ceramic Society 21 (2011) 1495–1498.
[35] K. Sutin, La-, K- and Nb-doped $0.90(Bi_{0.5}Na_{0.5}TiO_3)$–$0.10PbTiO_3$, Ceramics International 33 (2007) 1403–1407.
[36] C. Mourea, M. Villegasa, J.F. Fernándeza, P. Durána, Microstructural and piezoelectric properties of fine grained PZT ceramics doped with donor and/or acceptor cations, Ferroelectrics 127 (1992) 113–118.
[37] S.M. Hu, Nonequilibrium point defects and diffusion in silicon, Materials Science and Engineering R 13 (1994) 104–192.
[38] Y.F. Chang, Z.P. Yang, D.F. Ma, Z.H. Liu, Z.L. Wang, Phase transitional behavior, microstructure, and electrical properties in Ta-modified $[(K_{0.458}Na_{0.542})_{0.96}Li_{0.04}]$ NbO_3 lead-free piezoelectric ceramics, Journal of Applied Physics 104 (2008) 024109.
[39] Q. Xu, M. Chen, W. Chen, H.X. Liu, B.H. Kim, B.K. Ahn, Effect of CoO additive on structure and electrical properties of $(Na_{0.5}Bi_{0.5})_{0.93}Ba_{0.07}$-$TiO_3$ ceramics prepared by the citrate method, Acta Materialia 56 (2008) 642–650.